

Hysteresis and Noise from Electronic Nematicity in High Temperature Superconductors

E. W. Carlson,¹ K. A. Dahmen,² E. Fradkin,² and S. A. Kivelson^{3,4}

¹*Department of Physics, Purdue University, West Lafayette, Indiana 47907, USA*

²*Department of Physics, University of Illinois, Urbana, Illinois 61801, USA*

³*Department of Physics, Stanford University, Stanford, California 93105, USA*

⁴*Department of Physics and Astronomy, University of California, Los Angeles, California 90095, USA*

(Dated: November 13, 2018)

An electron nematic is a translationally invariant state which spontaneously breaks the discrete rotational symmetry of a host crystal. In a clean square lattice, the electron nematic has two preferred orientations, while dopant disorder favors one or the other orientations locally. In this way, the electron nematic in a host crystal maps to the random field Ising model (RFIM). Since the electron nematic has anisotropic conductivity, we associate each Ising configuration with a resistor network, and use what is known about the RFIM to predict new ways to test for electron nematicity using noise and hysteresis. In particular, we have uncovered a remarkably robust linear relation between the orientational order and the resistance anisotropy which holds over a wide range of circumstances.

PACS numbers: 72.70.+m, 74.25.Fy, 75.10.Nr

In the high temperature superconductors, in addition to superconductivity, there may exist various other types of order which break spatial symmetries of the underlying crystal, especially in the “pseudogap” regime at low doping.[1, 2, 3, 4, 5] However, it is often surprisingly difficult to obtain direct experimental evidence which permits one to clearly delineate in which materials, and in what range of temperature and doping, these phases occur. One such candidate order is the electronic nematic, which breaks orientational, but not translational, symmetry.[3] Orientational long range order (LRO) induces transport anisotropy, since it is easier to conduct along one direction of the electronic nematic than the other, and this is a natural way to look for nematic order. On the other hand, quenched disorder couples linearly to the order parameter, and so, for quasi-2D systems, will typically change a true thermodynamic transition into a mere crossover.

In this letter, we propose methods for detecting local electronic nematic order (nematicity) even in the presence of quenched disorder. We show that an electron nematic in a disordered square lattice maps to a random field Ising model (RFIM)[6] and that the transport properties of the system can be determined from a random resistor network whose local resistances reflect the local nematic transport anisotropy. In a host crystal such as the cuprates, an electron nematic (which may arise from local “stripe” correlations) tends to lock to favorable lattice directions, often either “vertically” or “horizontally” along Cu-O bond directions. The two possible orientations can be represented by an Ising pseudospin, $\sigma = \pm 1$, [7] and the tendency of neighboring nematic patches to align corresponds to a ferromagnetic interaction. In any given region, disorder due to dopant atoms between the cuprate planes produces electric field gradients which locally fa-

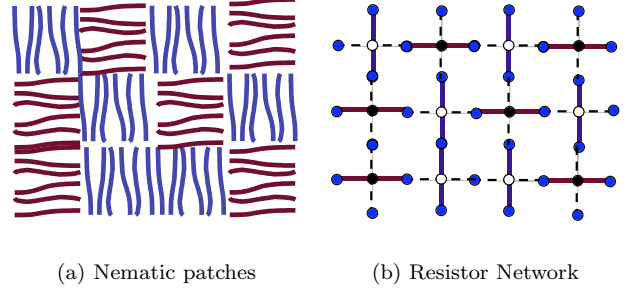


FIG. 1: Mapping of nematic patches to random resistor networks. (a) Configurations of nematic patches generated by the random field Ising model. (b) Corresponding resistor network, modeling local anisotropic conduction in each nematic patch. Solid lines are small resistors, and dotted lines are large ones.

vor one orientation or the other, and act like a random field on the electronic nematic, as illustrated in Fig. 1(a). Thus an electron nematic in a host crystal maps to the RFIM:

$$H = -J \sum_{\langle i,j \rangle} \sigma_i \sigma_j - \sum_i (h + h_i) \sigma_i \quad (1)$$

where $J > 0$ is the coupling between neighboring nematic patches. The local disorder field h_i is taken to be gaussian, with a disorder strength Δ characterized by the width of the gaussian distribution. The symmetry breaking field h may be produced by, *e.g.*, uniaxial strain, high current,[8] or magnetic field. For example, nematics can be aligned by an external magnetic field due to diamagnetic anisotropy, in which case $h \propto o(H^2)$. [9]

The macroscopic resistance anisotropy of a nematic[10,

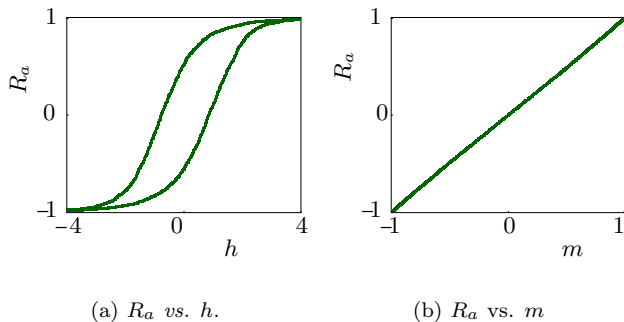


FIG. 2: Hysteresis and comparison of the macroscopic resistance anisotropy to the orientational order for size $L \times L = 100 \times 100$, disorder strength $\Delta = 3J$, temperature $T = 0$, microscopic resistance anisotropy $r = 2$, and external field sweep rate $\Omega = J/N$, where $N = L \times L$. (a) Hysteresis of the resistance anisotropy R_a (see text) *vs.* the symmetry breaking field h . (b) Resistance anisotropy R_a *vs.* orientational order parameter m . The resistance anisotropy is a remarkably good indicator of orientational order.

11, 12] transforms under rotations in the same way as the orientational order parameter $m = (1/N) \sum_i \sigma_i$ and is a natural candidate for measuring nematic order. The (normalized) resistance anisotropy is $R_a \equiv \left(\frac{r+1}{r-1} \right) \left(\frac{R_{xx} - R_{yy}}{R_{xx} + R_{yy}} \right)$, where $r \equiv R_{xx}^{\max}/R_{xx}^{\min}$ is the ratio of the extremal macroscopic resistances in the two fully oriented states. To obtain the transport properties, we map each pattern of local nematic orientations generated by Monte Carlo simulations of the RFIM (see Fig. 1(a)) to a resistor network (see Fig. 1(b)) which models the local anisotropic transport in each nematic patch. Each nematic patch (Ising pseudospin) becomes one node in the resistor network, with four surrounding resistors determined by the nematic orientation. For a “vertical” nematic patch, we assign the resistors to the “north” and “south” to be small, R_{small} , while the resistors to the “east” and “west” are large, $R_{\text{large}} = rR_{\text{small}}$. For a “horizontal” nematic patch, these assignments are reversed. When all patches are fully oriented so that $m \rightarrow 1$, the macroscopic resistance anisotropy must also saturate, $R_a \rightarrow 1$. More generally, in the thermodynamic limit $\langle R_a \rangle = mF(m, T, r)$, where F is an even function of m . Remarkably, as we will see below, $F = 1$ to a very good approximation and, under a wide range of circumstances, $\langle R_a \rangle \approx m$ throughout the entire range of m .

We use a Glauber update method to generate configurations of the RFIM, with periodic boundary conditions on the pseudospin lattice. The details of the algorithm are contained in Ref.[13]. We then calculate the resistance anisotropy R_a of the corresponding resistor network by the following method: For R_{xx} , we assign a uniform applied voltage to every site at the far left end of

the lattice, and a uniform ground to the far right end of the lattice, with open voltage boundary conditions in the y direction, corresponding to infinite resistors coming out of the top and bottom edges of the network. We then apply the bond propagation algorithm[14] to reduce the network to a single resistor equivalent to the macroscopic R_{xx} . R_{yy} is similarly calculated from the same starting resistor network, but with boundary conditions appropriate for R_{yy} .

Below a critical disorder strength, the 3D RFIM possesses a finite temperature phase transition to a low temperature ordered phase. However, in 2D the critical disorder is zero, and LRO is forbidden.[15] The quasi-2D case of coupled RFIM planes also has finite critical disorder,[16] but it is exponentially small. We focus here on two dimensions, and demonstrate that even in this case, where orientational LRO is forbidden, it is possible to detect the proximity to order through noise and hysteresis measurements.

We first present results at zero temperature, which exhibits the nonequilibrium behavior associated with hysteresis. Fig. 2 shows a simulation of the RFIM for a system of size $L = 100 \times 100$ at zero temperature. We present results for which the field h is incremented at a sweep rate $\Omega = J/N$, where $N = L \times L$ is the system size and $h = \Omega t$. In Fig. 2(a), we show a hysteresis loop for the resistance anisotropy R_a *vs.* the symmetry breaking field h , starting from the fully oriented state at $h = -\infty$. Fig. 2(b) plots R_a *vs.* m through one cycle of the hysteresis loop. The relationship is remarkably linear, and the macroscopic resistance anisotropy R_a shows precisely the same hysteretic behavior as m . This linear relation throughout the cycle is surprising, since for a given magnetization m not too close to 1, there are several values possible for the macroscopic resistance anisotropy. This is because the flow of current through the random resistor network depends not only on the relative concentration of “up” and “down” resistor nodes, but also on their spatial relation. In fact, for $m = 0$, R_a can take values between $\pm(r^2 - 1)/(r^2 + 6r + 1)$. However, for typical configurations generated by the RFIM, the main contribution to R_a is controlled by the number of up and down nodes, with their spatial relation being a small effect which goes to zero as the system size $L \rightarrow \infty$ or as $r \rightarrow 1$. (We do observe variations in R_a between configurations with the same magnitude of m at finite temperature or for small system sizes.) For the same reason, in confined geometries there can be more noise in the resistance anisotropy than is present in the true orientational order parameter. The fact that $\langle R_a \rangle \approx m$ over a wide range of parameters means that noise and hysteresis in this measurable property can be used to detect the electronic nematic.

Hysteresis subloops can be used to determine qualitatively the relative importance of interactions and disorder. Fig. 3 shows the behavior of subloops in the hysteresis curve of orientational order m *vs.* orienting field

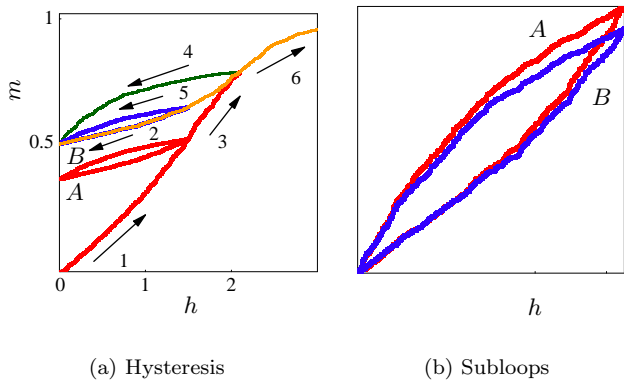


FIG. 3: (a) Field ramp-up from a disordered configuration at $T = 0$, with hysteresis subloops, for system size $L \times L = 100 \times 100$ and disorder strength $\Delta = 3J$. The arrows indicate the order in which the external field sweep is taken. Subloops A and B are both taken between the same extremal orienting fields $h = 1.5J$ and $h = 2.1J$, but with different histories. (b) Incongruency of subloops A and B, due to the presence of interactions. Here the orientational order parameter has been shifted to compare the shape of the two subloops. Subloop A, executed at lower m , has a higher slope than subloop B, executed at higher m .

h . Starting from zero field and a thermally disordered configuration, the field is swept up along path 1, then switched back along path 2 to take subloop A before continuing along path 3. Then path 4 begins a second subloop, within which path 5 begins subloop B, before continuing to raise the field through path 6 until m has saturated, $m \rightarrow 1$.

Notice that the subloops close, and also that once a subloop has closed, continuing to raise the field does not disturb the structure of the outer loop. This is indicative of return-point memory, a characteristic of the RFIM.[17] Additionally, subloops A and B in Fig. 3 are a comparison between the same two field strengths. The fact that the two are incongruent as shown in Fig. 3(b) indicates that interactions are present, and possibly even avalanches, *i.e.* that the hysteresis is not simply a linear superposition of elementary hysteresis loops of independent grains as in the Preisach model.[18, 19, 20] Here, we have used a disorder strength of $\Delta = 3J > \Delta_{crit}^{3D} = 2.16J$. At lower disorder, the subloops become narrower and difficult to resolve. Also, as temperature is increased, thermal disorder means that subloops become narrower, and no longer close precisely.

Recent magnetization measurements by Panagopoulos *et al.* [21, 22] on $\text{La}_{2-x}\text{Sr}_x\text{CuO}_4$ reveal hysteretic behavior reminiscent of the RFIM. Although some of the results look very similar to our Fig. 3, in fact our model does not explicitly include the ferromagnetic moments measured in this experiment. However, the small mag-

nitude of the measured magnetization may be consistent with ferromagnetic moments arising at defects in the local striped antiferromagnetic order of a nematic patch.

We now discuss equilibrium fluctuations. In confined geometries such as nanowires and dots, this model can exhibit telegraph noise in R_a due to thermal fluctuations of large correlated clusters. Recent transport experiments on underdoped YBCO nanowires by Bonetti *et al.*[23] reveal telegraph-like noise in the pseudogap regime. Using a YBCO nanowire of size $250\text{nm} \times 500\text{nm}$, they found that a time trace of the resistance at constant temperature $T=100\text{K}$ shows telegraph-like fluctuations of magnitude 0.25%, on timescales on the order of 50 seconds. These large scale, slow switches can be understood within our model as thermal fluctuations of a single correlated cluster of nematic patches. Individual nematic patches thermally fluctuating between two orientations also produce noise, but at higher frequency, and with smaller effect on the macroscopic resistance. By comparing the magnitude of the smallest typical resistance change to the resistance change at a telegraph noise event, one can estimate that the correlated cluster in the nanowire contains at least 5-6 nematic patches.

The nanowire represents a rather small system size when mapped to the RFIM. Neutron scattering experiments on the incommensurate peaks of underdoped YBCO indicate a coherence length of roughly 40nm. If we take this as an estimate of the size of one nematic patch (mapped to a single pseudospin in the RFIM), the nanowire is about 6×12 patches wide, and the effect of flipping a correlated cluster of pseudospins can dominate the response. In Fig. 4(a), we show a time series of R_{xx} in thermal equilibrium ($h = 0$) for a small system of size $L \times L = 6 \times 6$ at finite temperature with disorder strength $\Delta = 2J$, which is less than the 3D critical value. Notice the sizable thermal fluctuations in the macroscopic resistance. The high frequency noise is due to the thermal fluctuations of a single Ising pseudospin. The lower frequency telegraph noise, in which the resistance changes dramatically, is due to the correlated fluctuations of a cluster of pseudospins, in our case a cluster of 4 pseudospins. The histogram in Fig. 4(b) shows that the system switches between two main states.

In general, correlated clusters will thermally switch with a timescale which rapidly increases with their size. Confined geometries such as the nanowire are more likely to have a system-spanning cluster which causes slow, large scale noise. For larger system sizes, the histogram becomes smoother and can have multiple peaks. For systems larger than the Imry-Ma correlation length, large scale switches are highly unlikely. A probability distribution of size of cluster *vs.* frequency can be obtained from a histogram of the *differential resistance*, in which large scale switches will always be relegated to the tails of the distribution.

A further way to test for nematic patches is to measure

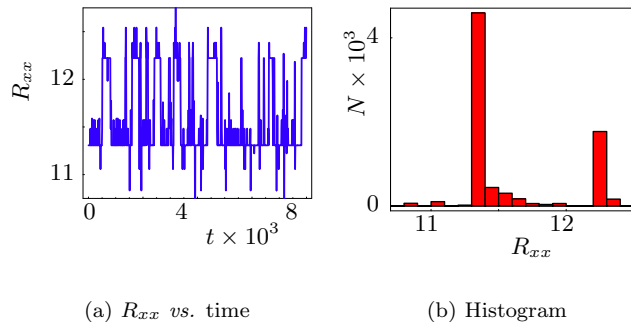


FIG. 4: (a) Telegraph noise in a confined geometry. Resistance R_{xx} vs. time of a small system of size $L \times L = 6 \times 6$ with disorder strength $\Delta = 2J$, at temperature $T = 0.5J$, in zero applied field, $H = 0$. An initial random state is allowed to thermalize for 10,000 MC steps before measurements are taken. The local microscopic conductivity anisotropy in the resistor network is $r = 2$. Small fluctuations are due to a single nematic patch fluctuating. Large switches are due to the thermal fluctuations of a single correlated cluster of nematic patches. (b) Histogram of the time series. N is the number of occurrences of a particular resistance. There are two main states, one for which the correlated cluster is “up”, and the other for which it is “down”.

cross correlations between the thermal noise in R_{xx} and R_{yy} as a function of time.[24] This can distinguish between macroscopic resistance fluctuations due to, *e.g.*, fluctuation superconductivity (which would cause *correlated* fluctuations of R_{xx} and R_{yy}), or due to RFIM-nematic physics (which would cause *anticorrelated* fluctuations).

This general method of connecting local anisotropic properties of an electronic nematic to macroscopic behavior can be extended to many experimental measurements. For example, applying an in-plane magnetic field should drive 4-fold symmetric incommensurate spin peaks in neutron scattering into a 2-fold symmetric pattern, in a hysteretic manner as the field is rotated from one Cu-O direction to the other. Superfluid density anisotropy should also display similar hysteresis with in-plane field orientation. Furthermore, the presence of correlated clusters in the RFIM has implications for STM. Whereas small correlated clusters have faster switching dynamics, large clusters are much slower,[18] so that different size clusters have different local power spectra. STM can be used to do *scanning noise spectroscopy*,[25] by measuring the power spectrum as a function of position, in order to produce a spatial map of correlated nematic clusters.

In conclusion, we have mapped the electron nematic in a host crystal to the random field Ising model. Using a further mapping to a random resistor network, we have predicted new ways to detect the electron nematic in disordered systems. We have demonstrated that the

macroscopic resistance anisotropy is a good measure of orientational order and is expected to display hysteresis and thermal noise characteristic of the random field Ising model. Recent experiments on noise in YBCO nanowires and hysteresis in LSCO exhibit behavior reminiscent of this model.

We thank T. Bonetti, D. Caplan, D. Van Harlingen, C. Panagopoulos and M. Weissman for many illuminating conversations which motivated this work and for sharing their unpublished work, and we thank T. Datta and J. C. Davis for helpful discussions. This work was supported in part through The Purdue Research Foundation (EWC), and by NSF grants DMR 03-25939 and DMR 03-14279 at UIUC, PHY 99-07949 at the KITP-UCSB (KAD), DMR 04-42537 at UIUC (EF), and DMR-04-21960 at Stanford and UCLA (SAK).

-
- [1] S. Kivelson, *et al.*, *Rev. Mod. Phys.*, **7**, 1201 (2003).
 - [2] E. W. Carlson, V. J. Emery, S. A. Kivelson, and D. Orgad, in *The Physics of Superconductors, Vol. II*, ed. J. Ketterson and K. Benneman, Springer-Verlag (2004).
 - [3] S. A. Kivelson, E. Fradkin, and V. J. Emery, *Nature*, **393**, 550 (1998).
 - [4] S. Chakravarty, R. B. Laughlin, D. K. Morr, and C. Nayak, *Phys. Rev. B*, **63**, 094503 (2001).
 - [5] C. M. Varma, *Phys. Rev. B*, **55**, 14554 (1997).
 - [6] T. Nattermann, in *Spin Glasses and Random Fields*, ed. A. Young, World Scientific, Singapore (1998).
 - [7] A. Abanov, V. Kalatsky, V. L. Pokrovsky, and W. M. Saslow, *Phys. Rev. B*, **51**, 1023 (1995).
 - [8] C. Reichhardt, C. J. Olson Reichhardt, and A. R. Bishop, to appear in *Europhys. Lett.*, cond-mat/0503261.
 - [9] P. Chaikin and T. Lubensky, *Principles of Condensed Matter Physics*, Cambridge University Press, Cambridge, UK (1995).
 - [10] E. Fradkin and S. A. Kivelson, *Phys. Rev. B*, **59**, 8065 (1999).
 - [11] K. B. Cooper, *et al.*, *Solid State Commun.*, **119**, 89 (2001).
 - [12] Y. Ando, K. Segawa, S. Komiya, and A. N. Lavrov, *Phys. Rev. Lett.*, **88**, 137005 (2002).
 - [13] R. A. White, A. Travesset, and K. A. Dahmen, Thermal effects on crackling noise, to be published.
 - [14] D. J. Frank and C. J. Lobb, *Phys. Rev. B*, **37**, 302 (1988).
 - [15] Y. Imry and S. K. Ma, *Phys. Rev. Lett.*, **35**, 1399 (1975).
 - [16] O. Zachar and I. Zaliznyak, *Phys. Rev. Lett.*, **91**, 036401 (2003).
 - [17] J. P. Sethna, *et al.*, *Phys. Rev. Lett.*, **70**, 3347 (1993).
 - [18] J. P. Sethna, K. A. Dahmen, and O. Perković, in *Science of Hysteresis*, ed. I. D. Mayergoyz and G. Bertotti, Academic Press, London (2004).
 - [19] M. P. Lilly, P. T. Finley, and R. B. Hallock, *Phys. Rev. Lett.*, **71**, 4186 (1993).
 - [20] I. D. Mayergoyz, *Mathematical Models of Hysteresis*, Springer-Verlag, Berlin (1991).
 - [21] C. Panagopoulos, M. Majoros, T. Nishizaki, and H. Iwasaki, cond-mat/0412570.
 - [22] C. Panagopoulos, M. Majoros, and A. Petrović, *Phys.*

- Rev. B*, **69**, 144508 (2004).
- [23] J. A. Bonetti, D. S. Caplan, D. J. Van Harlingen, and M. B. Weissman, *Phys. Rev. Lett.*, **93**, 087002 (2004).
- [24] R. D. Black, P. J. Restle, and M. B. Weissman, *Phys. Rev. Lett.*, **51**, 1476 (1983).
- [25] M. E. Welland and R. H. Koch, *App. Phys. Lett.*, **48**, 724 (1986).